Science of the Total Environment 958 (2025) 177826

Contents lists available at ScienceDirect

Science of the Total Environment

journal homepage: www.elsevier.com/locate/scitotenv

Short Communication

A preliminary study on the effects of rainfall-related conditions on chromium increase in ultramafic-hosted springs: A possible climate change concern?

Tiziano Boschetti [a,*], Stefano Segadelli [b], Francesca Gori [c], Gabriele Antolini [d], Lisa Bellini [e], Alessandra Raso [f], Enricomaria Selmo [a], Maurizio Barbieri [g], Paola Iacumin [a], Emilio Guidetti [f], Alessandro Gargini [e]

[a] Department of Chemistry, Life Sciences and Environmental Sustainability, University of Parma, Parco Area delle Scienze 157/a, 43124 Parma, Italy
[b] Geological Survey Emilia-Romagna Region, Viale della Fiera, 8, 40127 Bologna, Italy
[c] Department of Earth Sciences, Sapienza University of Rome, Piazzale Aldo Moro 5, 00185 Roma, Italy
[d] Regional Agency for Prevention, Environment and Energy of Emilia-Romagna, HydroMeteoClimate Service (ARPAE-SIMC), Viale Silvani 6, 40122 Bologna, Italy
[e] Department of Biological, Geological and Environmental Sciences — BiGeA, Alma Mater Studiorum University of Bologna, Via Zamboni 67, 40126 Bologna, Italy
[f] Montagna2000 SpA, Via Antonio Gramsci 8, 43043 Borgo Val di Taro, PR, Italy
[g] Department of Chemical Engineering and Environmental Materials, Sapienza University of Rome, via Eudossiana 18, 00184 Roma, Italy

HIGHLIGHTS

- Fall 2023 saw 4-day cumulative precipitation up to 300 mm in the Northern Apennine.
- Cr(III) concentration in ultramafic springs increase during heavy rainfall.
- Natural organic matter and Fe-minerals in debris may drive Cr(VI)-Cr(III) reduction.
- Cr(III) persists in aquifer due to wet-dry cycle effects and NOM-colloids stability.

GRAPHICAL ABSTRACT

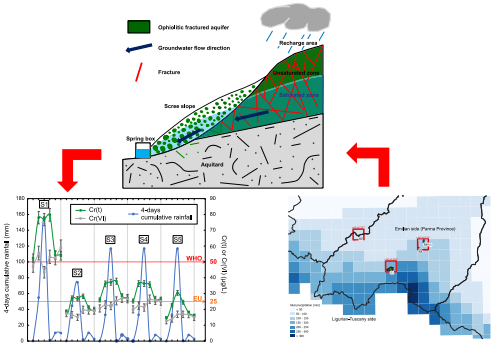

ARTICLE INFO

Editor: Christian Herrera

Keywords:
Ultramafic rock
Chromium
Springs
Groundwater
Cumulative precipitation

ABSTRACT

This study investigates the impact of intense rainfall on chromium concentrations in five springs discharging from ultramafic rocks in the Northern Apennines (Italy), which are used for drinking water supply through integration into the local water network. Total chromium concentration increased significantly in response to heavy rain, exceeding the WHO drinking water guideline value (up to 80 μg/L) in one spring and the forthcoming 2036 EU target of 25 μg/L in all the springs. This increase could be attributed to a synergistic combination of factors: i) the reduction of Cr(VI) to Cr(III) by natural organic matter (NOM) in soil and transport as NOM-Cr(III) colloids and/or during the oxidation of magnetite to ferrihydrite in the aquifer; ii) the abundance of detrital ultramafic material in the study area, which may store Cr(III)-bearing colloids too; iii) a triggering effect of first

* Corresponding author.
E-mail address: tiziano.boschetti@unipr.it (T. Boschetti).

https://doi.org/10.1016/j.scitotenv.2024.177826
Received 2 September 2024; Received in revised form 27 November 2024; Accepted 27 November 2024
Available online 11 December 2024

intense rainfall after a 20 dry consecutive days period (wet-dry cycle). Moreover, the persistence of a high Cr(III) concentration in the aquifer even a month after the intense rainfall event aligns with previous laboratory studies on NOM-Cr(III) colloidal stability, which showed that such colloids are highly stable and can persist in solution for at least 20 days.

1. Introduction

Ophiolitic outcrops are estimated to constitute approximately 2 ± 1 % of the Earth's crust, of which approximately 1 % comprises ultramafic rocks (Gwenzi, 2020; Scott et al., 2021). Despite their limited global distribution, ultramafic rocks in ophiolites can act as a significant chromium (Cr) source to water and soils, potentially leading to severe environmental degradation and health risks associated with drinking water sources. Trivalent chromium, Cr(III), predominantly exists in primary silicate minerals of serpentinized ultramafic rocks, such as spinel (chromite and picotite), pyroxene, and serpentine. In soils, secondary minerals, such as Fe(III)-(oxy)hydroxides and clays, are generally considered important hosts for Cr(III) because they can provide surface sites (via sorption) or structural sites (via isomorphic substitution) (Oze et al., 2004). However, Cr(III) is also present in fragments (clasts) of primary silicates or low-solubility hydroxides in soils conditions, such as $Cr(OH)_3$ or $Cr_xFe_{1-x}(OH)_3$, where it is considered substantially immobile (Kierczak et al., 2007). Cr(III) is primarily released from silicates during weathering and may be oxidized to Cr(VI) when adsorbed onto high-valence manganese oxides. Other efficient oxidants include H_2O_2, microbial metabolism, and photochemically generated radicals (Liang et al., 2021), while the kinetics of Cr(III) oxidation by O_2 from air or water are extremely slow in natural settings. Regardless of the mineralogical source and its oxidation processes, Cr(III) has low mobility in water because it is easily absorbable on mineral surfaces and solid-phase organic ligands (Focardi et al., 2013), whereas Cr(VI) is the dominant redox form in groundwater from ultramafic or alluvial aquifers consisting of clastic material from weathered rock.

Weathering processes in different climatic regions and lithological variations significantly influence Cr release and migration. However, although climate change may influence groundwater chemistry (Barbieri et al., 2023), the effects of heavy rainfall events on Cr still need to be explored. In polluted areas (with anthropogenic chromium), some studies (Dokou et al., 2016; Kumar and Riyazuddin, 2011) observed increases in both Cr(III) and Cr(VI) during arid or pre-monsoon periods, followed by a subsequent decrease in concentration after the rainfall events.

Ophiolites in the Northern Apennines are significant groundwater reservoirs and a primary public drinking water source (Segadelli et al., 2021). Locally, these aquifers cover areas ranging from 2 km^2 to 40 km^2, with thicknesses between 250 m and 600 m. From an environmental perspective, ophiolites also provide opportunities for applied scientific research, such as studying geochemical influences on habitats and identifying plant species resistant to toxic elements (Lombini et al., 1998).

In this study, the concentrations of total, Cr(t), and hexavalent, Cr (VI), chromium were analyzed in springs from ultramafic rocks in the Northern Apennines (Italy), with a focus on concentration changes before, during, and after two rainfall events that occurred during the rainy season of fall 2023. In this area and its surroundings, maximum precipitation indices and percentile-based indices suggest that extreme events have generally intensified since 1950, including a significant increasing trend in drought indices during the summer (Berényi et al., 2023).

2. Geological, hydrological, and climatological settings

The Northern Apennines is a fold-and-thrust belt that belongs to a collisional foreland basin system (Conti et al., 2020). Initially, the Northern Apennines formed as part of an accretionary wedge in response to the Late Cretaceous-Eocene closure of the Ligurian-Piedmont Ocean, subsequently evolving into a northeast-verging fold-and-thrust belt related to the west-verging subduction of the Adria plate beneath European plate and their Oligo-Miocene collision (Carmignani and Kligfield, 1990; Marroni et al., 2010). The ophiolite bodies present in the Alpine and Apennine belts are oceanic lithospheric remnants of the Ligurian-Piedmontese basin, which developed in the Middle to Upper Jurassic, separating the European plate from the Adria plate (Conti et al., 2020). In the Northern Apennines, ophiolites outcrop in two paleogeographic domains, which are identified based on their structural characteristics and their relationship with the associated sedimentary sequences (Conti et al., 2020) (Fig. 1, Supplementary Fig. SF1): the Internal and External Ligurides. Internal Ligurides contain peridotites, serpentinites, gabbros, and basalts, which form the bedrock of the Upper Jurassic-Paleocene sedimentary sequence deposits. Conversely, the External Ligurides contain ophiolitic sequences that occur as large slide blocks in Upper Cretaceous sedimentary mélanges (Conti et al., 2020). Numerous olistoliths of basalts and peridotites are embedded in the prevalent pelitic rock complexes of External Ligurides units, which represent the stratigraphic base of the Upper Cretaceous Helminthoid Flysch (Marroni et al., 2010) From the hydrogeological point of view, the main aquifers in the study area are serpentinized ultramafic (hard rock) aquifers occurring in Mt. Gorro (S1 spring), Mt. Gora (S2 spring), Mt. Zirone (S3 spring), and Mt. Prinzera (S4 and S5 springs) (Fig. 1). These ophiolitic bodies are mainly composed of fractured peridotites and bordered and underlain by low permeability deposits (aquitards) that are predominantly characterized by polygenic breccias made out of blocks of limestones or marly limestones inside a silty-clayey matrix (Segadelli et al., 2017). Various types of deposits with ultramafic composition (eluvium, colluvium, scree slope) or recent anthropogenic activities (quarry debris) characterize the study areas from the Quaternary period to the present (Supplementary Figs. SF2-SF6). These deposits show high infiltration capacity, provide an important regulating function in the natural aquifer recharge process, and feed some springs.

In such a hydrogeological setting, several perennial springs are located at the permeability threshold between the ophiolitic aquifers and the aquitard unit, often composed of clay-like materials. Therefore, springs can be classified as contact springs (Fetter and Kreamer, 2018). The hydroperiod of the sampled springs can be classified as perennial (continuous source year-round (Alfaro and Wallace, 1994). According to a previously proposed conceptual model, these springs represent the whole discharge of the aquifer units (Segadelli et al., 2021; Segadelli et al., 2017). The selected aquifers are of environmental and social interest, located in a natural reserve area, and exploited for drinking water supply by the local waterworks company (Montagna2000 Spa).

According to the Köppen-Geiger climate classification, in the period 1991–2020, the prevailing climate type in the study area is Temperate Oceanic Climate (Cfb), with an average annual temperature between 10 and 13 °C (11.6, 10.3, and 12.3 °C at the springs locations S1, S2, and S3-S5, respectively) and an average annual cumulative precipitation between 900 and 1400 mm (1316, 1040, and 911 mm at the springs locations S1, S2, and S3–5, respectively).

3. Methods

3.1. Field sampling and measurements

We planned each spring sampling round on the fourth and seventh days following the forecasted start of the rainfall event (note that both the start and end dates are counted when calculating days between two dates). The choice of the fourth day aligns with historical data; it corresponds to the delay observed in measuring a significant chromium increase in groundwater following a 60 mm rainfall event (Supplementary File SF10b). However, those data did not allow for further assessments since historical sampling was conducted on a monthly-basis (Supplementary File). Therefore, the seventh day following rainfall was chosen to check the persistence of dissolved chromium in the springs. In this study, based on weather forecasts consulted prior to sampling, rainfall events were predicted to start on October 20th and December 8th, 2023. Consequently, the first two sampling rounds were conducted on October 23rd and the 26th, respectively, while the second set of samplings occurred on December 11th and the 14th. A 'blank' sampling, i.e., supposed to be without rainfall influence, was conducted approximately 10–12 days before the forecasted rainfall events, specifically on October 12th and November 29th.

The data acquired in situ during each sampling and for each spring were: discharge, temperature, electrical conductance (EC), pH, and redox potential (Eh).

Spring discharge was measured using the volumetric method, often

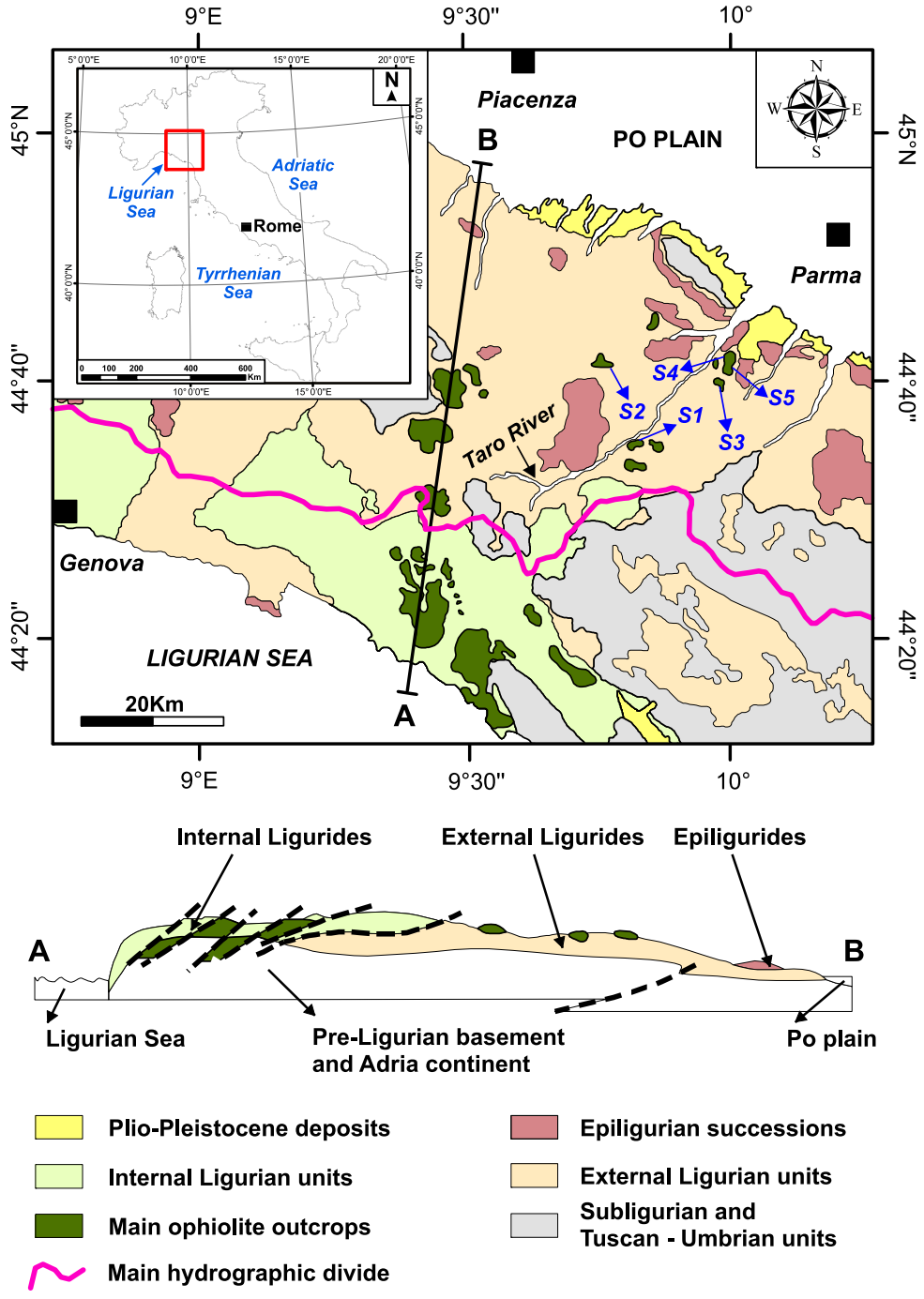

Fig. 1. Geological map and cross-section of the study area. S1-S5: location of the sampled springs.

with a flexible plastic bag, because the traditional bucket did not fit the outlet openings. According to Meinzer (1923), the obtained data were used for spring classification.

Labile physicochemical parameters were measured in situ using a portable multimeter (XS-PC 70 + DHS) to measure temperature (T), electric conductance (EC), and pH. The redox potential (Eh) was measured using a different multimeter (Thermo Scientific — Orion Star A121) with an ORP/Eh/Temp probe (Thermo Scientific — Orion 9179BNMD Triode), which was standardized before each measurement by an Eh = +420 mV solution (Thermo Scientific - Orion 967,961).

For each spring, we collected four different aliquots using double-cap PE bottles for laboratory analyses: three 100 mL bottles for anions, cations, and hexavalent chromium [Cr(VI)], respectively, and one 50 mL bottle for the stable isotope ratios of the water molecule. Before sampling, the bottles were conditioned in the laboratory using 1 % HNO_3 solution for one week, and then washed with Milli-Q® water (> 18.2 MΩ cm, Millipore). The water samples were filtered in the field using a 0.45 μm pore diameter polyamide (nylon) membrane filter with a quartz fiber prefilter (Whatman Polydisc GW). The first filtered water was used as the final wash of the bottles. After filling with filtered water, the 100 mL cations aliquots were acidified to 1 % *v*/v, adding 1 mL of 65 % HNO_3 Suprapur® (Supelco).

3.2. Laboratory analyses

The (bi)carbonate alkalinity, expressed as HCO_3^-, was analyzed by acidimetric titration using HCl, a digital titrator (SI Analytics TitroLine Easy), and methyl-orange as a dye indicator.

Two ion chromatographs (IC) were used to analyze the major anions Cl^-, SO_4^{2-}, F^-, and NO_3^- (Thermo Scientific Dionex ICS-5000) and major cations Ca^{2+}, Mg^{2+}, Na^+, and K^+ (Thermo Scientific Dionex ICS-1100).

According to the EPA method 7199 for Cr(VI) analysis (EPA, 1996), samples stored at 4 °C were analyzed within twenty-four hours of collection. Chromate as CrO_4^{2-} at 9.0 < pH < 9.5 was separated from sample solutions by an IC (Metrohm 930 Compact IC Flex), followed by a post-column derivatization using a 1,5-diphenylcarbazide, and detected at 530 nm by a spectrophotometer (Metrohm 944 UV/VIS Detector Vario) (EPA, 1996). The Cr(VI) results are the means of three replicates, and the standard deviation aligns with the eq. S = 0.059× + 1.055, where X is the mean Cr(VI) concentration of each sample (EPA, 1996).

The dissolved minor and trace ions Li, B, Al, Cr, Fe, Ni, As, Rb, Sr, Mo, Sn, Pb, Ba, Hg, and Pb were analyzed by an inductively coupled plasma mass spectrometer (ICP-MS; Thermo Scientific iCAP RQ) (Standard Method 3125) (Baird et al., 2017). Blanks, standard solutions, and sample dilutions were prepared using ultrapure water (Millipore Milli-Q® water, > 18.2 MΩ·cm). Although the analysis encompassed a more comprehensive range of elements, the ones listed above showed quantifiable concentrations in all the samples (LOD element list in Vincent, 2017; LOQ ≃ LOD x 10, according to Al-Hakkani, 2019). The chromium concentration obtained by ICP-MS corresponds to the total chromium in solution, i.e., Cr(t) = Cr(III) + Cr(VI). The KED (Kinetic Energy Discrimination) collision cell mode was used for Cr(t) measurements. It pressurizes the cell with a gas mixture and applies an energy discrimination barrier to delete unwanted polyatomic interferences. The analytical accuracy of this method ranges between 2 % and 5 % for all the analyzed elements. Quality control was performed by analyzing a blank and a standard reference material (SRM1640a, NIST, USA) after every tenth sample, treating them as samples. To account for uncertainties, regular laboratory replicates of samples were analyzed, and the instrument's precision and calibration were routinely verified using standard solutions.

The dissolved silica as SiO_2(aq) was analyzed using the heteropoly blue spectrophotometric method (Standard Method 4500-SiO2 D) (Baird et al., 2017), cuvette reagents test kit (Merck Millipore Spectroquant®) and a spectrophotometer (Merck Millipore PHARO 300 UV/VIS).

All methods conform to the QA/QC requirements of the Standard Methods (Standard Method 3020) (Baird et al., 2017).

The global anion-cation balance ≤5 % was checked on each sample (Standard Method 1030E for checking analyses' correctness) (Baird et al., 2017), considering not only major dissolved constituents as usual but also minor/trace elements, and utilizing the Phreeqc Interactive code (PhreeqcI) (Parkhurst and Appelo, 2013), version 3.7.3–15,968.

The stable isotope ratio of oxygen and hydrogen of the water molecule, $\delta^{18}O(H_2O)$ and $\delta^2H(H_2O)$, respectively, were determined by an automatic equilibration device (Finnigan HDO) in-line with a mass spectrometer (Finnigan Delta Plus) (Boschetti et al., 2005; Longinelli and Selmo, 2003). The $\delta^2H(H_2O)$ composition was obtained by equilibrating directly hydrogen gas H_2 with water using a platinum catalyst (Horita and Kendall, 2004), while the determination of $\delta^{18}O(H_2O)$ was performed on CO_2 gas equilibrated with the water at 18.0 ± 0.1 °C (GFL 1086 shaking water bath). All the samples were measured at least twice, and the reported value was the mean of two consistent results. All measurements were carried out against laboratory standards, periodically calibrated against the international isotope water standards recommended by the IAEA (V-SMOW2 and SLAP2) (Gröning, 2018). The standard error (2σ) was within ±0.08 to ±0.12 ‰ for $\delta^{18}O(H_2O)$ and ± 1 ‰ to ±2 ‰ for $\delta^2H(H_2O)$.

3.3. Thermodynamics and statistical calculations

The code PhreeqcI, combined with the Thermoddem (Blanc et al., 2012) thermodynamic dataset, version 1.1, was also used to calculate the activity of the dissolved constituents and saturation index of $Cr_xFe_{1-x}(OH)_3$ (Zhang et al., 2023). The same thermodynamic dataset was also used with the Act2 and Rxn tools of the software suite The Geochemist's Workbench® (GWB, version 12.0.9) (Bethke et al., 2022), which were used to calculate the $\log[Mg^{2+}/(H^+)^2]$ versus $\log[H_4SiO_4]$ activity diagram (Supplementary File SF8) and to check the thermodynamics of the reaction 1 in the Section 4.2, respectively. In comparison to a previous study (Boschetti and Toscani, 2008), the thermodynamic data of saponite-Mg-Fe^{3+}, vermiculite-Mg-Fe^{3+}, and p-antigorite (Apollaro et al., 2013; Blanc et al., 2021; Gunnarsson et al., 2005) were inserted in the Thermoddem database. The logK values for hydrolysis reactions of the aforementioned minerals were recalculated across a range of temperatures and pressures to maintain internal consistency between ions and solid phases in the database. The Principal Component Analysis (PCA) is a statistical tool that can discover unsuspected relationships that could reduce the dimensionality of the dataset while retaining the information present in the data structure. It has been successfully applied to explain the hydrogeochemical composition of groundwater in different geological settings (Awaleh et al., 2020; Barbieri et al., 2021; Boschetti et al., 2003). In this study, OriginPro version 2024b (OriginLab Corporation, Northampton, MA, USA) was used to extract the first two principal components using the correlation matrix. Physicochemical parameters, discharge, isotopes, and 4-days cumulative rainfall were selected as variables. The z-score standardization was applied to eliminate the different degrees of variation and the influence of size and dimension on variables with different units. The same software was also used for other statistical tests (ANOVA, Dunnet's Test, Cross Correlation Analysis), whereas The Joinpoint Regression Program (JRP), version 5.2.0.0 (April 2024; Statistical Methodology and Applications Branch, Surveillance Research Program, National Cancer Institute) and Weighted Bayesian Information Criterion (WBIC) were used to detect change point in the temporal series of chromium historical data (Supplementary File SF9a) (Barbieri et al., 2021).

3.4. Rainfall data

The climate data used in this study were extracted from Eraclito61 (https://dati.arpae.it/dataset/erg5-eraclito) (Antolini et al., 2016), a gridded climatological dataset obtained through spatial interpolation of

daily precipitation and min/max temperature, recorded at historical meteorological stations, on a regular grid of approximately 5 km resolution.

4. Results and discussion

All analysis results are reported in Supplementary Table 1 (Meinzer indices) and Table 2 (physicochemical, chemical, and isotope results).

4.1. Cumulative precipitation versus Cr concentration

During the rainy season of 2023 (October–December), we investigated the total chromium concentration, Cr(t) = Cr(III) + Cr(VI), and the concentration of only Cr(VI) in five Mg-HCO_3 springs discharging from three Northern Apennines (hard rock) aquifers formed by serpentinized ultramafic rocks. A detailed geochemical characterization of these springs is provided in the Supplementary File. The soil in these areas

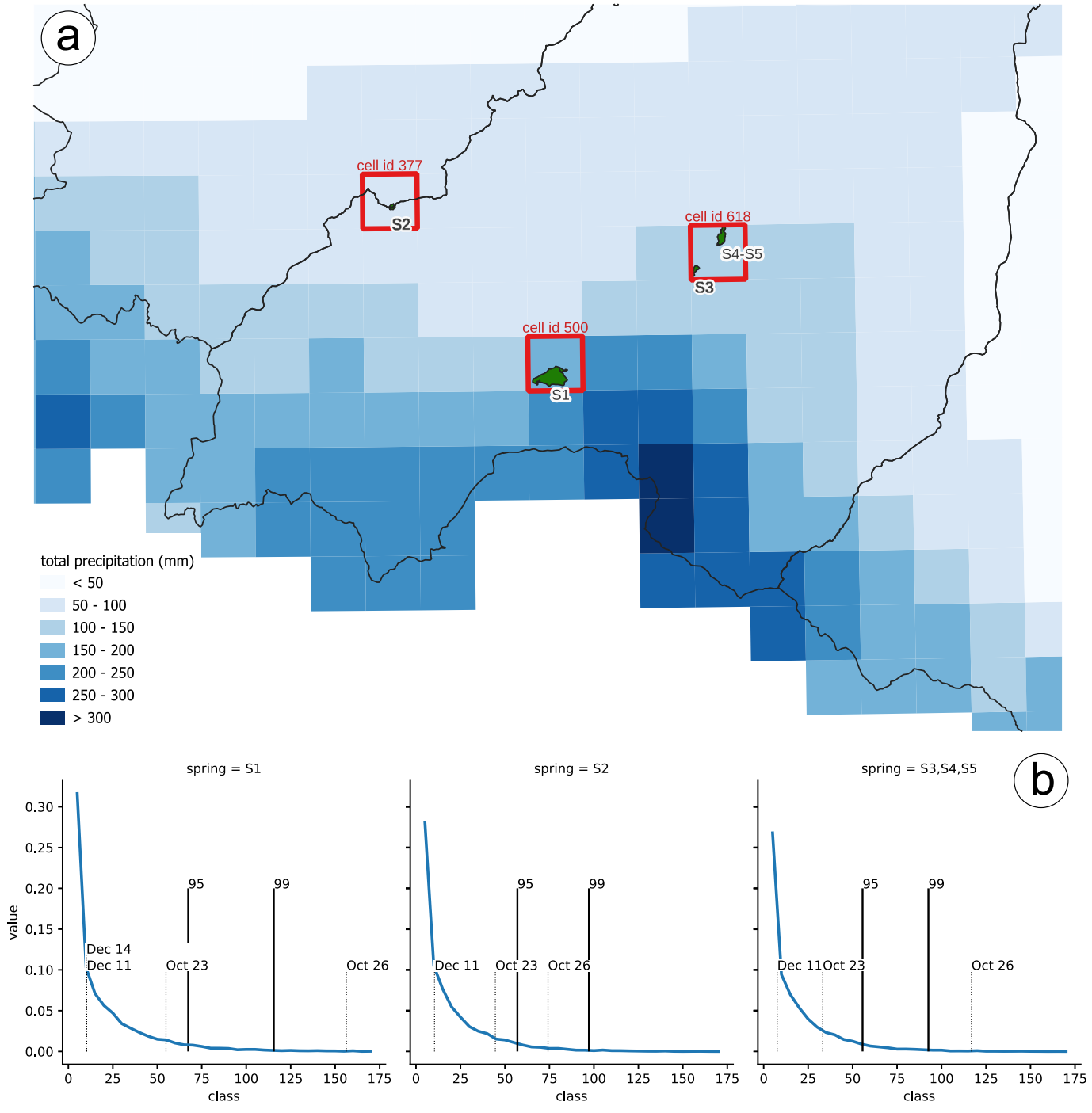

Fig. 2. a) Gridded total precipitation data for the event October 23–26, 2023. The black curve depicts province administrative boundaries (the southern limit coincides with the main hydrographic divide of the Northern Apennine (see also Fig. 1). The green areas represent the ophiolite aquifers that feed the S1-S5 springs. The red-contoured squares delimit the 5 km grid area (cell id #) of Eraclito61 from which climatic data were obtained (https://dati.arpae.it/dataset/erg5-eraclito) (Antolini et al., 2016). b) observed frequency distributions (1961–2023) of consecutive 4-days cumulative precipitation (blue line), with corresponding values of the 95th and 99th percentiles (black thick vertical lines), and the most relevant 4-days total precipitation events corresponding to the location of the sampled springs of this study (black dashed vertical lines) (events with total precipitation <5 mm, such as December 14th in S2 and S3-S5, are not reported).

contains significantly higher concentrations of geogenic Cr (up to 5000 ppm) than in the ultramafic rocks (up to 2500 ppm) (Venturelli et al., 1997).

A particularly intense convective precipitation event, generated by south-westerly humid air mass flows, took place on October 23–26th (most precipitation was observed for the area of interest between the 23rd and 24th), with cumulative values of over 300 mm close to the Apennine watershed (Fig. 2a), exceeding the 99th percentile of historical four-days cumulative precipitation at almost all rain gauges nearby the investigated springs (Fig. 2b). In particular, the total precipitation for this event is higher (much higher for spring S1) than the 99th percentile for all springs except for spring S2, for which it is lower than 99th but higher than 95th percentile.

The six sampling rounds conducted before and after that rainfall event showed an increase in Cr(t) followed by a decrease, mirroring the trend of cumulative precipitation (Fig. 3a). The Cr(VI) concentration, typically the dominant dissolved Cr-species in these waters, was indistinguishable from Cr(t) at the beginning and end of the event. However, during the three sampling rounds in the proximity of the peak of rainfall, Cr(t) significantly exceeds Cr(VI) (Fig. 3a). Therefore, the Cr(t) increment is mainly due to Cr(III), which jumps from 10 to 40 % (Fig. 3b).

The Dunnett's test (Fig. 3c; Supplementary Table 3) made after a One-Way ANOVA for repeated measures also showed that the Cr(III) concentrations measured on October 26th were not significantly different from those on October 23rd and November 29th. However, it was in comparison to October 12th, December 11th, December 14th. Therefore, increases in Cr(III) were observed not only during the peak of the high rainfall event, which occurred on October 26th, but also during the first day of that event (October 23rd) and after one month after the event (November 29th). The early Cr(t)/Cr(III) increase before October 26th is likely attributable to the dry period preceding the high rainfall event. Laboratory studies have demonstrated that the wet–dry cycle affects soil by inducing internal reduction reactions (Chen et al., 2024), leading to: i) the reduction of Cr(VI) to Cr(III), ii) alteration of the binding of Cr ions to soil particles, impacting chromium migration; iii) the involvement of microorganisms in chemical processes that consume organic matter. Accordingly, the high rainfall event in October 2023 followed a dry period that had lasted for at least 24 consecutive days and occurred before the event of October 23rd (Eraclito61 dataset for the sites in Fig. 2). On the other hand, the delayed decrease in Cr(III) in the days following the rainfall event is likely due to the slow change of Cr (III)-favorable physicochemical conditions. Indeed, the Eh measured in the springs (0.30 ± 0.09 V) is significantly lower than the value calculated for the Cr(VI)-Cr(III) redox equilibrium (0.42 ± 0.03 V) (Two-Way ANOVA, page 9 of the Supplementary File; Supplementary Table 2). Specifically, the lowest value is very similar to that calculated for the N (V)-N(III) equilibrium (0.35 ± 0.01 V) (Supplementary File; Supplementary Table 1), likely activated in the vadose waters and soil during

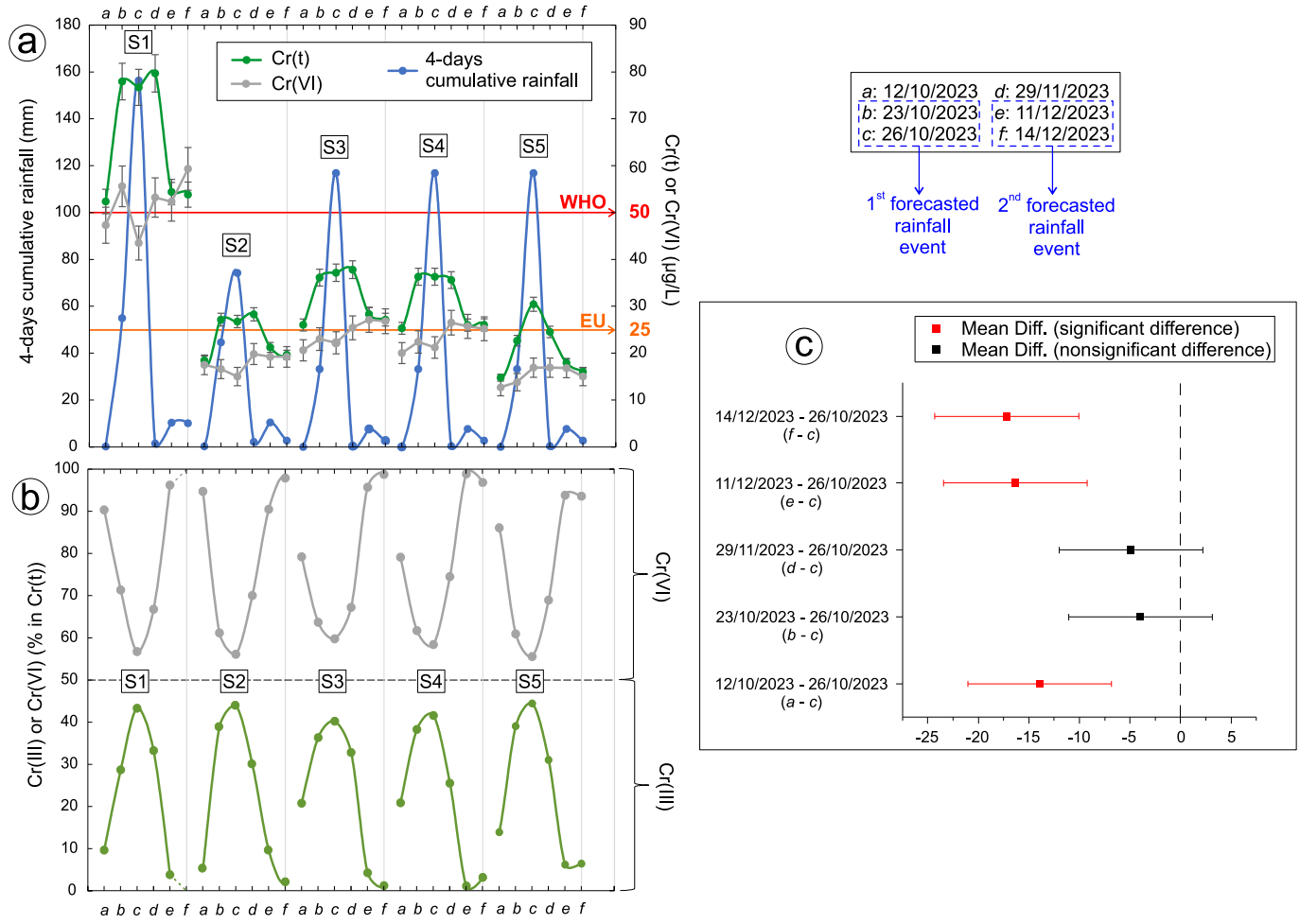

Fig. 3. a) Comparison of variations in total chromium, Cr(t), hexavalent chromium, Cr(VI), and four-day cumulative rainfall in the spring's area (Fig. 1; Fig. 2) during the six sampling rounds of the S1–S5 springs (a–f data as day/month/year). The red and orange horizontal arrows depict the WHO and forthcoming 2036-EU drinking guideline values for Cr(t): 50 µg/L (WHO, 2022) and 25 µg/L (EU, 2020), respectively. b) Relative percentage variations of trivalent, calculated as Cr(III) = Cr(t) - Cr(VI), and Cr(VI) in the sampled springs. c) Significance of the multiple comparisons (Dunnet's Test) performed on Cr(III) concentrations (control factor: October 26th, alias *c* sampling).

dissimilatory nitrate reduction to ammonium by bacteria and organic matter dissolved by rainfall (Chen et al., 2024; Friedl et al., 2018). In addition to its strong redox capabilities, the recycling of natural organic matter (NOM) during wet-dry cycles could also explain the most probable transport mechanism of Cr(III). This most likely occurs in the form of Cr(III)-bearing NOM colloids (1–220 nm), which can easily move through porous media (Li et al., 2022; Li et al., 2020; Liao et al., 2020). These colloids could also account for the persistence of the high Cr(III) signal in the sampled groundwater after the end of the rainfall event. Indeed, colloidal stability studies suggest that Cr(III)-HA-Fe colloids (HA = humic acid) are highly stable and persist for at least 20 days without substantial change in particle size (Liao et al., 2020). Finally, although the acidic pH of rainwater (5.4 under present-day atmospheric CO_2 partial pressure) can enhance Cr(III) mobility in alkaline soils, this would be generally restricted to near neutral pH values, i.e., the mean pH of the samples in this study, because at that values the precipitation of polymeric Cr(III)-hydroxides become rapid (Zhitkovich, 2011). However, if the NOM contribution is relatively high, Cr(III) mobility in the form of NOM-Cr(III) colloids can still occur at these pH levels (Andjelkovic et al., 2012; Chen et al., 2024).

4.2. Processes controlling changes in Cr concentration

Principal component analysis (PCA) clearly distinguishes the five sample clusters according to their respective spring location (Fig. 4) (Supplementary Table 4). All sampled waters are fresh (Total Dissolved Solids TDS < 1 g/L), with the samples from the S1 spring having the highest salinity (mean TDS = 0.37 ± 0.01 g/L), which likely drove the direct relationships among most of the analyzed chemical parameters in the PCA. Cr(t) concentrations were also the highest for that spring, reaching up to 80 μg/L from Oct-23rd to Nov-29th, thereby exceeding the current drinking water guideline values of 50 (WHO, 2022) (a target of 25 μg/L is to be met by 2036) (EU, 2020). Notably, such a high value coincides with the peak of cumulative rainfall (Fig. 1a). Moreover, the Cr (t) variable vector is directly associated with the isotopic composition of the water molecule (Fig. 2). This might appear coincidental, especially considering that the S1 spring showed the highest mean isotope values but no significant variations in isotope composition, which was seen only in S5 spring (Supplementary Fig. SF9). The more ^{18}O- and ^{2}H-enriched isotope values of S1, in comparison to the mean values of the other springs, could be attributed to S1's closer proximity to the Northern Apennines ridge (Fig. 1, Fig. 2). Large-scale atmospheric disturbances from the southwestern sector (the Ligurian Sea and the Ligurian-Tuscany side of the Northern Apennines; Fig. 2), which are more frequent during the rainy (autumn and winter) months, would discharge their rainfall loads near the ridge. Conversely, at lower elevations on the northeastern Emilian side, precipitation —and consequently the recharged spring discharge— tends to be more depleted. Indeed, higher (heavier) isotopic values result from orographic precipitation events. In contrast, convective and other precipitation events produce lower (lighter) isotopic values, where the vapor mass becomes progressively depleted by rainout processes (Rhodes et al., 2021). As a consequence, the rainout process leads to precipitation at the end of a rain event with more negative isotope values than at the onset (Clark, 2015). This process explains the difference in the mean isotope composition between springs located near (S1) or far (S2–S5) from the

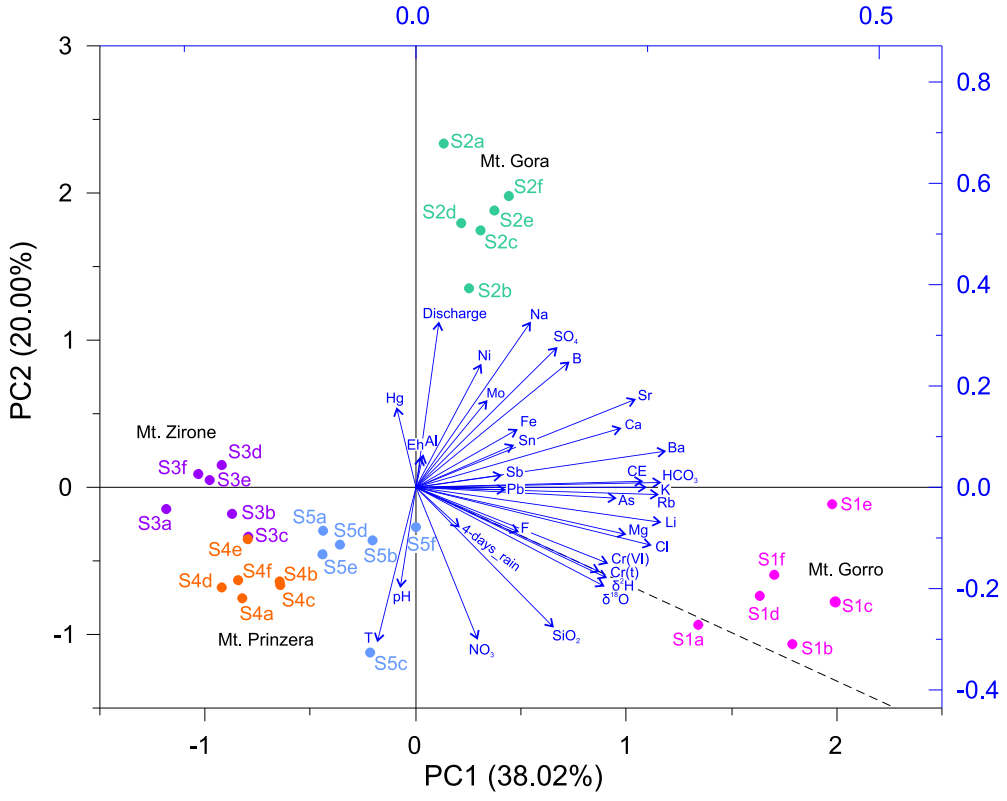

Fig. 4. Biplot of the first two principal components (PC1 and PC2, explaining 38.02 % and 20.00 % of the variance, respectively; Supplementary Table 4) from the PCA of the physicochemical parameters, isotope ratios, and cumulative precipitation values in the area of the sampled springs. The biplot displays both the variable loadings (eigenvectors, blue arrows; coordinates on the top and right axes) and the sample scores (colored dots labeled with letters a-f representing the sampling dates, as seen in Fig. 1; coordinates on the bottom and left axes). The spring samples cluster into three main groups corresponding to their ultramafic aquifer units. In particular, the Mt. Zirone (S3) and Mt. Prinzera (S4-S5) springs are closely grouped within the same climatic cell, used to extract the four days of cumulative precipitation (Fig. 2a). Co-linear variable vectors indicate strong positive correlation, with the vector length proportional to the variable influence on the PC score. Sample proximity to a vector reflects variable influence on the sample. Overlapping Cr(t) and δ^2H vectors (dashed line) highlight their strong positive correlation, particularly pronounced in S1 samples due to the intense rainfall event on October 23–26th, 2023.

Northern Apennines' main divide. It also accounts for the higher standard deviation observed in both isotope and discharge (highest Meinzer index, Supplementary Table 1) values at the S5 spring, which could be related to a huge unconsolidated ultramafic scree slope aquifer (Supplementary Figs. SF5-SF6).

In Fig. 4, the vector of the variable related to the four days of cumulative precipitation amount is close to the dissolved silica content, a key parameter for this type of water. Indeed, on an activity diagram using $\log[SiO_2aq]$ and the ratio $\log[Mg^{2+}]/[H^+]^2$ as variables, the degree of evolution of water–rock interactions can be indicated (Supplementary Fig. SF8). In this context, the samples from spring S1, which have a higher chromium content, also show higher values of the activity ratios. It is, therefore, intuitive to hypothesize that a higher evolutionary degree of interactions with the mineral paragenesis of the serpentinized ultramafites corresponds to a higher Cr(t) content when compared to the other less evolved groundwater flow systems. However, the differences in the evolutionary degree of water–rock interactions among the various springs can only explain the differences in the mean or median Cr(t) content, given that the latter is usually represented by Cr(VI), but not the specific Cr(III) increases related to rainfall. Therefore, it is likely that the variations observed during rainfall could be due to several processes not necessarily related to dissolved silica: i) the mobilization of Cr(III) adsorbed by secondary minerals coating the weathering surfaces of ultramafic rock fragments and soil particles (colloids); ii) a persistent Cr (VI)-Cr(III) reduction also driven by Fe(II)- to Fe(III)-bearing mineral oxidation as magnetite to ferrihydrite, locally present in a widespread manner (Boschetti and Toscani, 2008):

$$\underset{\text{magnetite}}{Fe^{(II)}Fe_2^{(III)}O_4} + 0.6667H^+ + 4.333H_2O + 0.3333Cr^{(VI)}O_4^{2-} = \underset{\text{ferrihydrite}}{3Fe^{(III)}(OH)_3} + 0.3333HCr^{(III)}O_{2(aq)} \quad (1)$$

Accordingly, the reaction proceeds from left to right, as verified by thermodynamic calculation ($\Delta G_r < 0$) using the activities of water and ions from the spring waters and combining different solid species (i.e., amorphous or crystalline magnetite and 2-line or 6-line ferrihydrite) (Supplementary Table 5). After that, the post-rainfall drop in Cr(III), and Cr(t), concentration is likely driven and buffered by the $Fe_xCr_{1-x}(OH)_3$ supersaturation and precipitation (Dai et al., 2016; He and Traina, 2005) (Supplementary Table 5).

Alternatively, the increase in chromium could be attributed to the upwelling from greater depths of more geochemically evolved waters with lower redox potentials, driven by a strengthened piston flow caused by the heavy rain (Sugiyama et al., 2018). However, this seems unlikely, at least for the deepest and most evolved hyperalkaline waters from ultramafites. Indeed, that kind of water does not contain detectable chromium, and a significant increase in pH should also be observed, given their OH-dominant composition (Boschetti et al., 2013; Boschetti and Toscani, 2008). Instead, the ultramafic bodies in the study area are characterized by the presence of ultramafic natural and anthropogenic debris (Jafarian and Jafarian, 2017; Oze et al., 2003), the latter produced by the intense excavation activities for extracting building stone materials (Supplementary Figs. SF2-SF6). It has been observed in other locations that the overflow of ultramafic debris from quarry activity releases large quantities of chromium, especially during heavy rain events (Gunkel-Grillon et al., 2014). In the study area, this is demonstrated by a re-examination of historical data on the chromium content of water in groundwater from two piezometer boreholes, one located outside a quarry area and the other inside. While the former showed no significant differences between Cr(t) and Cr(VI) levels, the latter exhibited significantly higher Cr(t) content during rainy season monitoring (Supplementary Fig. SF10a). Cross-correlation analysis was employed to determine if the debris influence hypothesis applies to the current sample set. Recognizing that the number of samples might not be sufficient to meet the minimum requirements for this type of analysis (McGee, 2000), the results highlight a significant correlation between the cumulative rainfall over 4 days and Cr(III) content, specifically in springs S2 and S5 (Fig. 5), where ultramafic debris is more extensive or forms a vast part of the aquifer structure (Fig. SF3; Figs. SF5-SF6). The non-significance of the other sites suggests the need for more frequent or extended sampling due to excessive white noise.

5. Conclusions

The present study shows that an increase in total chromium in ultramafic aquifers can be triggered by climate-related factors, specifically intense rainfall following dry periods. Further analyses are undoubtedly needed, such as increasing the sampling frequency during rainy periods to allow more meaningful time series analyses, performing targeted filtration/ultrafiltration to assess the impact of NOM-Cr(III)-Fe colloids, and analyzing the organic matter content in soils and dissolved in water. Groundwater in the study areas is crucial for the local population, who rely on it for drinking water. Currently, local efforts to address the issue of dissolved chromium in groundwater are focused on Cr(VI), with ex-situ treatment conducted before the water is introduced into the aqueduct network. These measures include mixing with water containing negligible Cr(VI) levels or treating the water by removing Cr(VI) with a chelating resin. Therefore, the Cr(III) increase in groundwater during

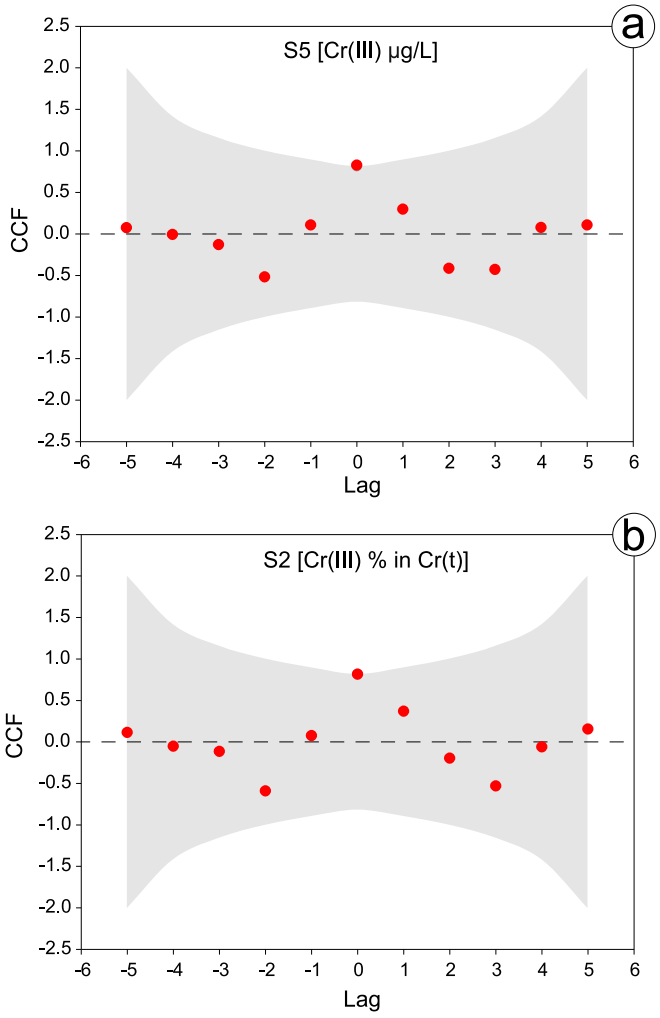

Fig. 5. Cross-correlation function (CCF) at different lag values (red dots) between Cr(III) in mg/L (S5, a-diagram) or Cr(III) as a percentage in Cr(t) (S2, b-diagram) versus the 4-days cumulative rainfall time series. In both diagrams, the correlation is significant at Lag = 0, as the CCF exceeds the 95 % confidence band limit (red gray area): 0.829 > 0.816 (a-diagram) and 0.817 > 0.816 (b-diagram), respectively.

and after heavy rainfall events, as evidenced in this study, could be considered harmless compared to the carcinogenic nature of Cr(VI) (WHO, 2022). It is worth noting, however, that while many studies classify Cr(III) as an essential trace element (Monga et al., 2022; Swaroop et al., 2019), other studies emphasize its potential risks (Brown et al., 2024; Vincent, 2017). This highlights the need for further epidemiological studies to establish two differentiated concentration thresholds for the two species, and the importance of long-term monitoring to track variations in their concentrations in drinking water. Additional concerns might arise from the drinking-water treatment, as: i) Cr(III) can be oxidized to Cr(VI) during the chlorination of drinking water (Lindsay et al., 2012), and ii) climate model projections indicate an increase in extreme events in the future (Madsen et al., 2014). Finally, further studies on local health risk assessment are also needed to evaluate the actual health risk to the population and identify effective measures to mitigate contamination. On a global scale, in areas where ultramafic aquifers are used for water supply networks, these processes must be carefully monitored to mitigate potential health risks.

CRediT authorship contribution statement

Tiziano Boschetti: Writing – review & editing, Writing – original draft, Visualization, Validation, Supervision, Software, Methodology, Investigation, Data curation, Conceptualization. **Stefano Segadelli:** Writing – review & editing, Writing – original draft, Visualization, Validation, Supervision, Methodology, Investigation, Formal analysis, Data curation, Conceptualization. **Francesca Gori:** Methodology, Formal analysis, Data curation. **Gabriele Antolini:** Writing – review & editing, Writing – original draft, Validation, Supervision, Investigation, Data curation, Conceptualization. **Lisa Bellini:** Formal analysis, Data curation. **Alessandra Raso:** Methodology, Funding acquisition, Formal analysis, Data curation. **Enricomaria Selmo:** Funding acquisition, Data curation. **Maurizio Barbieri:** Validation, Supervision. **Paola Iacumin:** Supervision, Formal analysis. **Emilio Guidetti:** Project administration, Funding acquisition. **Alessandro Gargini:** Visualization, Validation, Resources, Project administration, Investigation, Funding acquisition, Conceptualization.

Declaration of competing interest

The authors declare that they have no known competing financial interests or personal relationships that could have appeared to influence the work reported in this paper.

Acknowledgments

We thank the three anonymous reviewers for their thoughtful reviews, insightful comments, and helpful suggestions. Their feedback has significantly improved the final version of this manuscript.

Appendix A. Supplementary data

Supplementary data to this article can be found online at https://doi.org/10.1016/j.scitotenv.2024.177826.

Data availability

all the data used for the study are uploaded as supplementary file or available upon request

References

Alfaro, C., Wallace, M., 1994. Origin and classification of springs and historical review with current applications. Environ. Geol. 24, 112–124.
Al-Hakkani, M.F., 2019. Guideline of inductively coupled plasma mass spectrometry "ICP-MS": fundamentals, practices, determination of the limits, quality control, and method validation parameters. Sn Applied Sciences 1.
Andjelkovic, D.H., Andjelkovic, T.D., Nikolic, R.S., Purenovic, M.M., Blagojevic, S.D., Bojic, A.L.J., et al., 2012. Leaching of chromium from chromium contaminated soil-a speciation study and geochemical modelling. Journal Serbian Chemical Society 77, 119–129.
Antolini, G., Auteri, L., Pavan, V., Tomei, F., Tomozeiu, R., Marletto, V., 2016. A daily high-resolution gridded climatic data set for Emilia-Romagna, Italy, during 1961-2010. Int. J. Climatol. 36, 1970–1986.
Apollaro, C., Marini, L., Critelli, T., De Rosa, R., 2013. The standard thermodynamic properties of vermiculites and prediction of their occurrence during water-rock interaction. Appl. Geochem. 35, 264–278.
Awaleh, M.O., Boschetti, T., Adaneh, A.E., Daoud, M.A., Ahmed, M.M., Dabar, O.A., et al., 2020. Hydrochemistry and multi-isotope study of the waters from Hanlé-Gaggadé grabens (Republic of Djibouti, East African Rift System): A low-enthalpy geothermal resource from a transboundary aquifer. Geothermics 86.
Baird, R.B., Eaton, A.D., Rice, E.W., 2017. Standard Methods for Examination of Water and Wastewater, 23rd edition. American Public Health Association, American Water Works Association, Water Environment Federation, Washington D.C.
Barbieri, M., Franchini, S., Barberio, M.D., Billi, A., Boschetti, T., Giansante, L., et al., 2021. Changes in groundwater trace element concentrations before seismic and volcanic activities in Iceland during 2010-2018. Sci. Total Environ. 793.
Barbieri, M., Barberio, M.D., Banzato, F., Billi, A., Boschetti, T., Franchini, S., et al., 2023. Climate change and its effect on groundwater quality. Environ. Geochem. Health 45, 1133–1144.
Berényi, A., Bartholy, J., Pongrácz, R., 2023. Analysis of precipitation-related climatic conditions in European plain regions. Weather and Climate Extremes 42.
Bethke, C.M., Farrell, B., Yeakel, S., 2022. The Geochemist's Workbench® Release 12 - GWB Essentials Guide. Aqueous Solutions, LLC, Champaign, IL.
Blanc, P., Lassin, A., Piantone, P., Azaroual, M., Jacquemet, N., Fabbri, A., et al., 2012. Thermoddem: a geochemical database focused on low temperature water/rock interactions and waste materials. Appl. Geochem. 27, 2107–2116.
Blanc, P., Gherardi, F., Vieillard, P., Marty, N.C.M., Gailhanou, H., Gaboreau, S., et al., 2021. Thermodynamics for clay minerals: calculation tools and application to the case of illite/smectite interstratified minerals. Appl. Geochem. 130.
Boschetti, T., Toscani, L., 2008. Springs and streams of the Taro-Ceno valleys (northern Apennine, Italy): reaction path modeling of waters interacting with serpentinized ultramafic rocks. Chem. Geol. 257, 76–91.
Boschetti, T., Cortecci, G., Bolognesi, L., 2003. Chemical and isotopic compositions of the shallow groundwater system of Vulcano Island, Aeolian archipelago, Italy: an update. GeoActa 2, 1–34.
Boschetti, T., Venturelli, G., Toscani, L., Barbieri, M., Mucchino, C., 2005. The Bagni di Lucca thermal waters (Tuscany, Italy): an example of Ca-SO_4 waters with high Na/Cl and low Ca/SO_4 ratios. J. Hydrol. 307, 270–293.
Boschetti, T., Etiope, G., Pennisi, M., Romain, M., Toscani, L., 2013. Boron, lithium and methane isotope composition of hyperalkaline waters (northern Apennines, Italy): terrestrial serpentinization or mixing with brine? Appl. Geochem. 32, 17–25.
Brown, S., Marchi, S., Thomas, C.S., Hale, A.R., Lockart, M., Bowman, M.K., et al., 2024. Forming a chromium-based interstrand DNA crosslink: implications for carcinogenicity. J. Inorg. Biochem. 251.
Carmignani, L., Kligfield, R., 1990. Crustal extension in the northern Apennines - the transition from compression to extension in the Alpi Apuane Core complex. Tectonics 9, 1275–1303.
Chen, Z., Chen, Y., Liang, J., Sun, Z., Zhao, H., Huang, Y., 2024. The release and migration of Cr in the soil under alternating wet–dry conditions. Toxics 140.
Clark, I., 2015. Groundwater Geochemistry and Isotopes. Taylor & Francis Group, Sound Parkway NW, Boca Raton FL.
Conti, P., Cornamusini, G., Carmignani, L., 2020. An outline of the geology of the northern Apennines (Italy), with geological map at 1:250,000 scale. Ital. J. Geosci. 139, 149–194.
Dai, C., Zuo, X.B., Cao, B., Hu, Y.D., 2016. Homogeneous and heterogeneous (Fe_x, Cr_{1-x})$(OH)_3$ precipitation: implications for Cr sequestration. Environ. Sci. Technol. 50, 1741–1749.
Dokou, Z., Karagiorgi, V., Karatzas, G.P., Nikolaidis, N.P., Kalogerakis, N., 2016. Large scale groundwater flow and hexavalent chromium transport modeling under current and future climatic conditions: the case of Asopos River basin. Environ. Sci. Pollut. Res. 23, 5307–5321.
EPA, 1996. Method 7199 - determination of hexavalent chromium in drinking water, groundwater, and industrial wastewater effluents by ion chromatography. SW-846: Test Methods for Evaluating Solid Waste, Physical/Chemical Methods. Environ. Prot. Agency 10.
EU, 2020. Directive (EU) 2020/2184 of the European Parliament and of the Council of 16 December 2020 on the quality of water intended for human consumption (recast).
Fetter, C.W., Kreamer, D., 2018. Applied Hydrogeology, Fifth edition. Waveland Press, Inc., Long Grove, IL, USA.
Focardi, S., Pepi, M., Focardi, S., 2013. Microbial reduction of hexavalent chromium as a mechanism of detoxification and possible bioremediation applications. In: Chamy, R., Rosenkranz, F. (Eds.), Biodegradation - Life of Science. InTech, Croatia.
Friedl, J., De Rosa, D., Rowlings, D.W., Grace, P.R., Müller, C., Scheer, C., 2018. Dissimilatory nitrate reduction to ammonium (DNRA), not denitrification dominates nitrate reduction in subtropical pasture soils upon rewetting. Soil Biol. Biochem. 125, 340–349.
Gröning, M., 2018. TEL Technical Note No. 03 - stable isotope internal laboratory water standards: Preparation, calibration and storage. In: International Atomic Energy Agency - IAEA, Vienna, Austria, p. 12.
Gunkel-Grillon, P., Laporte-Magoni, C., Lemestre, M., Bazire, N., 2014. Toxic chromium release from nickel mining sediments in surface waters. New Caledonia. Environmental Chemistry Letters 12, 511–516.

Gunnarsson, I., Arnorsson, S., Jakobsson, S., 2005. Precipitation of poorly crystalline antigorite under hydrothermal conditions. Geochim. Cosmochim. Acta 69, 2813–2828.
Gwenzi, W., 2020. Occurrence, behaviour, and human exposure pathways and health risks of toxic geogenic contaminants in serpentinitic ultramafic geological environments (SUGEs): a medical geology perspective. Sci. Total Environ. 700.
He, Y.T., Traina, S.J., 2005. Cr(VI) reduction and immobilization by magnetite under alkaline pH conditions: the role of passivation. Environ. Sci. Technol. 39, 4499–4504.
Horita, J., Kendall, C., 2004. Stable isotope analysis of water and aqueous solutions by conventional dual-inlet mass spectrometry. In: De Groot, P.A. (Ed.), Handbook of Stable Isotope Analytical Techniques. 1. Elsevier, Amsterdarm, The Netherlands, pp. 1–37.
Jafarian, A., Jafarian, S., 2017. Geogenic and anthropogenic chromium contamination in groundwater in an ophiolitic area, northeastern Iran. Universal Journal of Geoscience 5, 183–190.
Kierczak, J., Neel, C., Bril, H., Puziewicz, J., 2007. Effect of mineralogy and pedoclimatic variations on Ni and Cr distribution in serpentine soils under temperate climate. Geoderma 142, 165–177.
Kumar, A.R., Riyazuddin, P., 2011. Chromium speciation in a contaminated groundwater: redox processes and temporal variability. Environ. Monit. Assess. 176, 647–662.
Li, B.R., Liao, P., Xie, L., Li, Q.Q., Pan, C., Ning, Z.G., et al., 2020. Reduced NOM triggered rapid Cr(VI) reduction and formation of NOM-Cr(III) colloids in anoxic environments. Water Res. 181.
Li, B.R., Liao, P., Liu, P., Wang, D.J., Ye, Z.H., Wang, J.F., et al., 2022. Formation, aggregation, and transport of NOM-Cr(iii) colloids in aquatic environments. Environmental Science-Nano 9, 1133–1145.
Liang, J.L., Huang, X.M., Yan, J.W., Li, Y.Y., Zhao, Z.W., Liu, Y.Y., et al., 2021. A review of the formation of Cr(VI) via Cr(III) oxidation in soils and groundwater. Sci. Total Environ. 774.
Liao, P., Pan, C., Ding, W.Y., Li, W.L., Yuan, S.H., Fortner, J.D., et al., 2020. Formation and transport of Cr(III)-NOM-Fe colloids upon reaction of Cr(VI) with NOM-Fe(II) colloids at anoxic-oxic interfaces. Environ. Sci. Technol. 54, 4256–4266.
Lindsay, D.R., Farley, K.J., Carbonaro, R.F., 2012. Oxidation of Cr^{III} to Cr^{VI} during chlorination of drinking water. J. Environ. Monit. 14, 1789–1797.
Lombini, A., Dinelli, E., Ferrari, C., Simoni, A., 1998. Plant-soil relationships in the serpentinite screes of Mt. Prinzera (northern Apennines, Italy). J. Geochem. Explor. 64, 19–33.
Longinelli, A., Selmo, E., 2003. Isotopic composition of precipitation in Italy: a first overall map. J. Hydrol. 270, 75–88.
Madsen, H., Lawrence, D., Lang, M., Martinkova, M., Kjeldsen, T.R., 2014. Review of trend analysis and climate change projections of extreme precipitation and floods in Europe. J. Hydrol. 519, 3634–3650.
Marroni, M., Meneghini, F., Pandolfi, L., 2010. Anatomy of the Ligure-Piemontese subduction system: evidence from late cretaceous-middle Eocene convergent margin deposits in the northern Apennines, Italy. International Geology Review 52, 1160–1192.
McGee, M., 2000. Power analysis and sample size determination for well-known time series models. In: Yaffee, R.A. (Ed.), Introduction to Time Series Analysis and Forecasting with Applications of SAS and SPSS. Academic Press, Inc., Sea Harbor Drive Orlando, FL, United States, pp. 481–493.
Meinzer, O.E., 1923. Outline of Ground-Water Hydrology - with Definitions, vol. 494. United States Government Printing Office, Washington DC, USA.
Monga, A., Fulkea, A.B., Dasguptab, D., 2022. Recent developments in essentiality of trivalent chromium and toxicity of hexavalent chromium: implications on human health and remediation strategies. Journal of Hazardous Materials Advances 7.
Oze, C.J., LaForce, M.J., Wentworth, C.M., Hanson, R.T., Bird, D.K., Coleman, R.G., 2003. Chromium geochemistry of serpentinous sediment in the Willow core, Santa Clara County, CA. U.S. Department of Interior, U.S. Geological Survey, Reston, VA, p. 24.
Oze, C., Fendorf, S., Bird, D.K., Coleman, R.G., 2004. Chromium geochemistry in serpentinized ultramafic rocks and serpentine soils from the Franciscan Complex of California. Am. J. Sci. 304, 67–101.
Parkhurst, D.L., Appelo, C.A.J., 2013. Description of input and examples for PHREEQC version 3 - a computer program for speciation, batch-reaction, one-dimensional transport, and inverse geochemical calculations. Book 6. U.S. Geological Survey Techniques and Methods 497.
Rhodes, A.L., Guswa, A.J., Newell, S.E., 2021. Using stable isotopes to identify orographic precipitation events at Monteverde, Costa Rica. In: Bruijnzeel, L.A., Scatena, F.N., Hamilton, L.S. (Eds.), Tropical Montane Cloud Forests - Science for Conservation and Management. Cambridge University Press United Kingdom of Great Britain and Northern Ireland.
Scott, A., Oze, C., Shah, V., Yang, N., Shanks, B., Cheeseman, C., et al., 2021. Transformation of abundant magnesium silicate minerals for enhanced CO_2 sequestration. Communications Earth & Environment 2.
Segadelli, S., Vescovi, P., Ogata, K., Chelli, A., Zanini, A., Boschetti, T., et al., 2017. A conceptual hydrogeological model of ophiolitic aquifers (serpentinised peridotite): the test example of Mt. Prinzera (northern Italy). Hydrol. Process. 31, 1058–1073.
Segadelli, S., Filippini, M., Monti, A., Celico, F., Gargini, A., 2021. Estimation of recharge in mountain hard-rock aquifers based on discrete spring discharge monitoring during base-flow recession. Hydrgeol. J. 29, 949–961.
Sugiyama, A., Masuda, S., Nagaosa, K., Tsujimura, M., Kato, K., 2018. Tracking the direct impact of rainfall on groundwater at Mt. Fuji by multiple analyses including microbial DNA. Biogeosciences 15, 721–732.
Swaroop, A., Bagchi, M., Preuss, H.G., Zafra-Stone, S., Ahmad, T., Bagchi, D., 2019. Benefits of chromium(III) complexes in animal and human health. In: Vincent, J.B. (Ed.), The Nutritional Biochemistry of Chromium (III). Elsevier, Amsterdam, Netherlands; Oxford, United Kingdom; Cambridge, MA, pp. 251–278.
Venturelli, G., Contini, S., Bonazzi, A., Mangia, A., 1997. Weathering of ultramafic rocks and element mobility at Mt. Prinzera, northern Apennines, Italy. Mineral. Mag. 61, 765–778.
Vincent, T., 2017. Thermo Scientific iCAP RQ ICP-MS: Typical Limits of Detection. A Technical Note. TN43427-EN 0117. Thermo Fisher Scientific.
WHO, 2022. Guidelines for Drinking-Water Quality: Fourth Edition Incorporating the First and Second Addenda. World Health Organization, Geneva.
Zhang, S.N., Cheng, L., Zuo, X.B., Cai, D.W., Tong, K., Hu, Y.D., et al., 2023. (Fe, Cr)(OH) 3 Coprecipitation in solution and on soil: roles of surface functional groups and solution pH. Environ. Sci. Technol. 57, 7516–7525.
Zhitkovich, A., 2011. Chromium in drinking water: sources, metabolism, and cancer risks. Chem. Res. Toxicol. 24, 1617–1629.